

Profusion of Transition Pathways for Interacting Hysterons

Martin van Hecke^{1,2}

¹*AMOLF, Science Park 104, 1098 XG Amsterdam, Netherlands*

²*Huygens-Kamerlingh Onnes Lab, Universiteit Leiden,
P.O. Box 9504, NL-2300 RA Leiden, Netherlands*

(Dated: April 30, 2023)

The response, pathways and memory effects of cyclically driven complex media can be captured by hysteretic elements called hysterons. Here we demonstrate the profound impact of hysteron interactions on pathways and memory. Specifically, while the Preisach model of independent hysterons features a restricted class of pathways which always satisfy return point memory, we show that three interacting hysterons generate more than 15,000 transition graphs, with most violating return point memory and having features completely distinct from the Preisach model. Exploring these opens a route to designer pathways and information processing in complex matter.

A rugged landscape governs the intermittent response of complex materials, which features sequences of transitions between metastable states that constitute pathways [1–18]. Under cyclical driving, these pathways form hysteresis loops which may encode Return Point Memory (RPM), the widespread ability of complex materials to revisit a previous state when the driving reaches a previous extremal value [15–21]. Microscopically, localized bistable entities such as spins or rearranging zones play a crucial role [13, 15, 19–23]. These can be modeled as *hysterons*, two-state elements which switch between phases "0" and "1" when the global driving field U passes through the upper and lower "bare" switching fields u_i^+ or u_i^- (Fig. 1) [13, 15–21, 24–27]. Indeed, collections of non-interacting hysterons—the well-studied Preisach model—describe surprisingly complex sequences of transitions and satisfy RMP [13, 16, 17, 20, 21, 27].

Here we probe the rich physics of interacting hysterons. Interactions are to be expected [13, 17, 22, 25, 26] and while non-interacting hysterons switch their phases independent of each other, in sequences determined by the order of their bare switching fields, interactions scramble and entangle these switching orders. To characterize the response of coupled hysterons we use transition graphs (t-graphs), a recently introduced representation that captures all pathways of a complex system and aids in probing memory effects [13, 20–27]. We show that interactions mushroom the number of t-graphs, which feature transitions (avalanches, pseudo-avalanches, multi-edges) and topological structures (subharmonic cycles, breakdown of RPM) completely distinct from the Preisach model. Besides providing a fresh perspective on the response of complex media, we show that our study paves the way for materials with designer pathways [27–31].

Model. — We investigate t-graphs of n interacting hysterons. We model interactions via a linear dependence of the switching fields U_i^\pm of hysteron i on the phases s_j of all other hysterons (Fig. 1):

$$U_i^{+,-}(S) = u_i^{+,-} - \sum_{j \neq i} c_{ij} s_j, \quad (1)$$

where S denotes the state $\{s_1, s_2, \dots\}$ and $u_i^{+,-}$ and c_{ij}

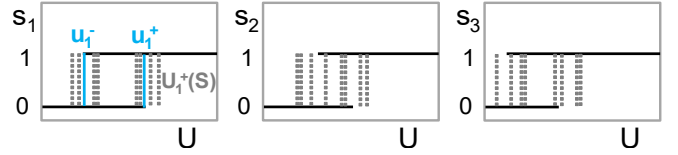


FIG. 1. (color online) Hysteresis diagrams for three interacting hysterons driven by a global field U . A single hysteron features internal phase $s_i = 0, 1$ and bare switching fields $u_i^{+,-}$ (blue, full line). Interactions lead to multiple state-dependent switching fields $U_i^{+,-}(S)$ (grey, dashed) for each hysteron.

are the bare switching fields and interactions constants [25, 26]. We take $0 < u_i^- < u_i^+ < 1$, choose a gauge where $c_{ii} = 0$ [32], and require $u_1^+ > u_2^+ > \dots$ [20, 21, 33]. Each state S becomes unstable when U exceeds $U^+(S)$ or decreases below $U^-(S)$, thus initiating an up or down transition (extremal states have one transition). Interactions can induce avalanches that proceed via intermediate, unstable states. For example, consider the case where S initially transitions to a state S' at value of U where S' is not stable, and then transitions to a stable landing state S'' . We call this an avalanche of length two, denote it as $S \rightarrow S''$, and ignore the intermediate states which in experiments would not be observable.

Transition graphs. — We collect all transitions between states that can be reached from the extremal states $\mathbf{0} = \{0, 0, \dots\}$ or $\mathbf{1} = \{1, 1, \dots\}$ into a t-graph via an iterative algorithm. Starting from state $\{\mathbf{0}\}$, we determine its up transition and landing state, and then iteratively determine the transitions from all fresh landing states, until no new states can be found (see Supplemental Information). The resulting t-graph contains all N nodes that are reachable from the extremal states and $2N - 2$ directed edges which represent the transitions, where each edge is labeled by its character (up or down), its critical field U^+ or U^- , and the number of intermediate steps.

T-graph construction involves evaluating "design" inequalities on the parameters which govern each transition. These inequalities are not independent and vary

strongly with the t-graph topology. Moreover, certain parameters, in particular for strong interactions, may yield avalanches that return to their initial state (self-loops), or contain states where more than one hysteron is unstable; we consider the corresponding t-graphs ill-defined. Together, this makes finding and classifying all t-graphs complex (see Supplemental Information).

Two interacting hysterons.— We determine all possible t-graphs for two interacting hysterons by exhaustively sampling the parameter space span by the four bare switching fields $u_i^{+,-}$ and two coupling coefficients c_{12} and c_{21} (Fig. 2). Without interactions, there are only two distinct t-graphs (Fig. 2(a)-2(b)), selected by the sign of $u_1^- - u_2^-$ [20, 21]. For antiferromagnetic interactions, where $c_{ij} \leq 0$ and the flipping of hysteron j from $0 \rightarrow 1$ suppresses the flipping of hysteron i from $0 \rightarrow 1$, we obtain three additional t-graphs which feature avalanches ($\{01\} \rightarrow \{10\}$) of length two (Fig. 2(c)-2(e)), while for purely ferromagnetic interactions ($c_{ij} \geq 0$), there are four additional t-graphs featuring avalanches $\{00\} \rightarrow \{11\}$ (Fig. 2(f)-2(i)). For interactions of mixed sign, two additional t-graphs that both feature pseudo-avalanches of length three occur (Fig. 2(j)-2(k))— e.g., the transition $\{00\} \rightarrow \{10\}$ in t-graph (j) proceeds via intermediate states $\{01\}$ and $\{11\}$. Finally, for strong coupling, approximately 6% of parameters yield ill-defined t-graphs. We conclude that interactions yield qualitatively new transitions and increase the number of t-graphs.

We have sampled the probability for each t-graph to occur as a function of C (ensemble size 10^8), for the ‘mixed interaction’ case where $|c_{ij}| \leq C$ (Fig. 2(l)). These probabilities grow and decay as powerlaws $\sim C_i^{n_i}$ for small and large C , with integer exponents n_i . This is because some of the design inequalities are ‘critical’ and require the fine tuning of parameters when c_{ij} is large or small. For example, the specific condition $u_2^+ - u_1^+ > -c_{12}$ is ‘critical’: as $u_2^+ < u_1^+$, the difference between u_1^+ and u_2^+ must be less than c_{12} when $c_{12} \downarrow 0$, which has a probability of $\mathcal{O}(|c|)$. The number of independent critical conditions controls n_i (Supplemental Information).

Our data shows that all t-graphs can be realized for arbitrary weak interactions. This can be understood from the invariance of the t-graph topology under shifts of the switching fields and multiplications of all parameters: The t-graph for $\bar{c}_{ij} = \lambda c_{ij}$, $\bar{u}_i^\pm = \lambda(u_i^\pm + 1/\lambda)$ maintains its topology for arbitrarily small interaction constants ($\lambda \rightarrow 0$). Hence, weak interactions can break the Preisach phenomenology when the switching fields are close to each other.

A plethora of t-graphs.— The number and qualitative diversity of t-graphs mushrooms with n . We determined t-graphs for 10^8 systems of $n = 3$ hysterons for $C = 1$ (Fig. 3). Strikingly, we obtain more than 15,000 distinct t-graphs. We stress that in absence of interactions, there are only $n!$ distinct t-graphs [20, 21].

We now contrast the characteristic features of these t-

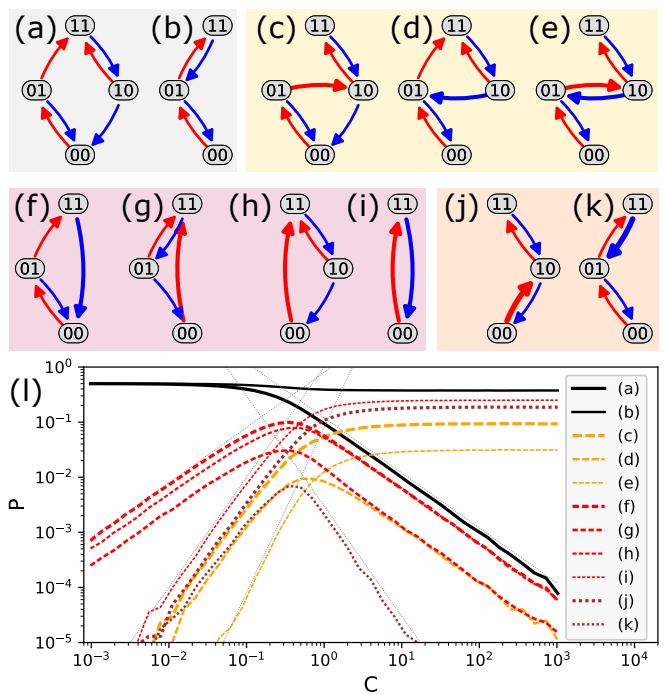


FIG. 2. Distinct transition graphs for $n = 2$ coupled hysterons, where up and down transitions are represented by red and blue arrows respectively. (a-b) For $c_{ij} = 0$ we recover the well-known Preisach t-graphs [20, 21]. (c-e) For $c_{ij} < 0$, ‘horizontal’ avalanches of length two (thick arrows) may occur. (f-i) For $c_{ij} > 0$, four additional t-graphs with vertical avalanches may occur. (j-k) For c_{ij} of mixed sign, two additional t-graphs featuring pseudo-avalanches of length three (thick arrows) are observed. (l) Probability of each t-graph as function of magnitude of the interactions C ; fractions are for well-defined cases only. Thin grey lines indicate integer powerlaw scalings.

graphs to those of the Preisach model (see Supplemental Information):

(i) *Scrambling.*— We first focus on t-graphs without avalanches (Fig. 3(a)-3(c)). In the Preisach model, the switching order is independent of state, and we define two non-avalanche transitions as scrambled when they are inconsistent with such a state-independent ordering. For example, the t-graph in Fig. 3(a) contains the scrambled pair of transitions $\{011\} \rightarrow \{001\}$ and $\{111\} \rightarrow \{110\}$ which evidences hysteron interactions.

(ii) *Avalanches.*— Without interactions, each transition corresponds to a single hysteron switching its phase, but in the presence of interactions many t-graphs feature avalanches where more than one hysteron changes phase simultaneously (Fig. 3(d)-3(f)).

(iii) *Dissonance.*— In the Preisach model, up and down transitions lead to the increase, respectively decrease of the magnetization $m(\mathbf{s}) := \sum_i s_i$. Remarkably, interactions allow for *dissonant* avalanches, where an up (down) avalanche leads to a decrease (increase) of the

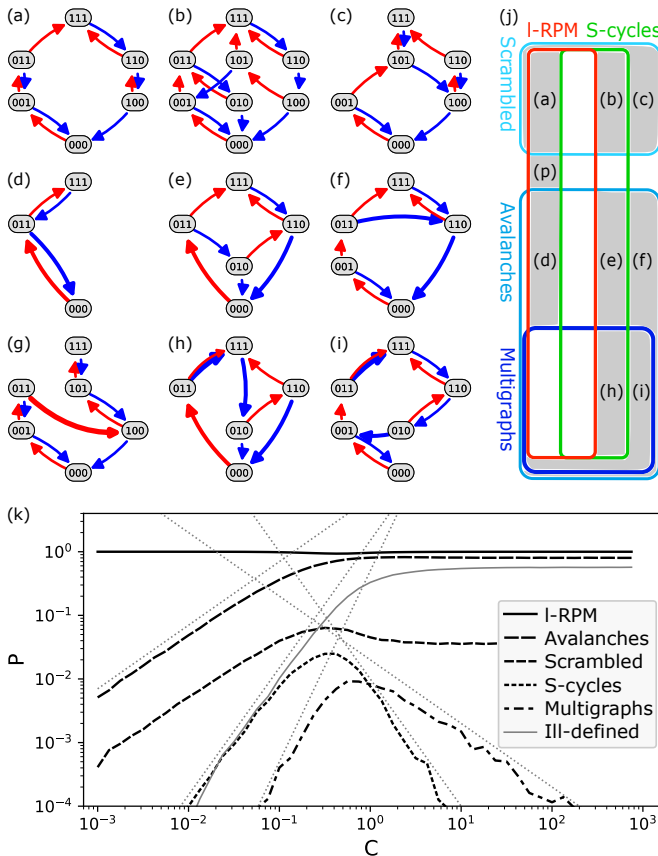


FIG. 3. (a-c) Examples of scrambled t-graphs, featuring either I-RPM (a), a subharmonic-cycle (b), or neither (c). (d-f) Examples of t-graphs with avalanches (thick arrows), featuring either I-RPM (d), a subharmonic-cycle (e), or neither (f). (g) t-graph featuring a dissonant avalanche. (h-i) Multi-graphs with (h) and without (i) a subharmonic cycle. For details, see Supplemental Information. (j) Venn-diagram for properties of $n = 3$ t-graphs; letters refer to the examples in earlier panels, while Preisach t-graphs are indicated by '(p)'. (k) Probabilities of $n = 3$ t-graph types, where $c_{ij} \in [-C, C]$. These probabilities grow and decay as integer power-laws (dashed lines). While scrambling, S-cycles, and multigraphs most likely arise for intermediate interactions, the fraction of t-graphs featuring avalanches increases with C and plateaus at 80%. The fraction of parameters that yield ill-defined t-graphs also increases with C and plateaus at 57%; fractions are for well-defined cases only.

magnetization (Fig. 3(g)).

(iv) *Multi-graphs*.— Interactions lead to cases where two states are connected both by an up and down transition—e.g., a pair of 'horizontal' avalanches that both preserve the magnetization, or an ordinary transition paired with a dissonant avalanche. The t-graphs then become directed *multigraphs* (Fig. 3(h)-3(i)).

(v) *Subharmonic cycles*.— In the Preisach model, the t-graphs feature a hierarchical loop-within-loop structure which precludes the presence of subharmonic cy-

cles (S-cycles) [20, 21]. Interactions allow for such S-cycles, where under cyclic driving the system revisits earlier states only after more than one driving cycle; for example, the t-graph of Fig. 3(b) contains an S-cycle $\{001\} \uparrow \{011\} \uparrow \{111\} \downarrow \{110\} \downarrow \{100\} \uparrow \{101\} \downarrow \{001\} \dots$ where \uparrow and \downarrow denote up and down transitions.

(vi) *Breakdown of loop-Return Point Memory*.— Finally, the t-graphs in the Preisach model all satisfy loop-Return Point Memory (l-RPM). A t-graph satisfies l-RPM when one cannot escape a subloop without the driving passing through some previously established extremal values [20, 21]. While ferromagnetic interactions preserve l-RPM [17, 20, 21], we find that antiferromagnetic interactions can break l-RPM; for example, in Fig. 3c the transitions $\{100\} \rightarrow \{110\} \rightarrow \{111\}$ escape the subloop between nodes $\{000\}$ and $\{101\}$.

In summary, interactions generate a host of new features of the t-graphs: Property (i) breaks the correlation between transitions of the Preisach model, properties (ii)-(iv) enlarge the types of transitions between states, and properties (v)-(vi) enlarge the possible global topologies of t-graphs.

We have also explored purely antiferromagnetic interactions, which yield over 4,000 distinct t-graphs which cover all t-graph classes of Fig. 3j, but do not feature dissonant avalanches [34]. In contrast, purely ferromagnetic interactions yield slightly less than 200 t-graphs, do not generate S-cycles, multigraphs or dissonant avalanches and only produce t-graphs that satisfy l-RPM (possibly with "vertical" avalanches) [16-21]. Hence, while antiferromagnetic interactions are essential to obtain exotic behavior, mixed interactions produce the largest variety of t-graphs.

Statistics.— We have sampled the probability of l-RPM, avalanches, scrambling, S-cycles, multi-graphs and ill-defined cases as function of C (ensemble size 10^5). While the majority of parameters yield t-graphs that satisfy l-RPM (minimum fraction ~ 0.93 for $C \approx 0.4$), more than 62% of distinct t-graphs breaks l-RPM. Hence, while a fraction of all t-graphs dominates the statistics (see Supplemental Information), interactions produce a wide variety of t-graphs.

Designer Pathways.— We suggest that the complex pathways of interacting hysterons naturally can be described in the language of computing. In particular, the directed graphs that encode sequential computations in finite state machines [35] are strongly reminiscent of t-graphs, where the labels of each edge ("up transition at $U = 0.5$ ") play the role of the input to the "hysteron machine".

As a first example, we explore dissonant avalanches to realize t-graphs that contain all eight state in a single pathway of up transitions. In our dataset, 740 realizations representing 51 distinct t-graphs contain such pathways. We select an "ADC" example where both the up and down pathways between $\mathbf{0}$ and $\mathbf{1}$ follow the or-

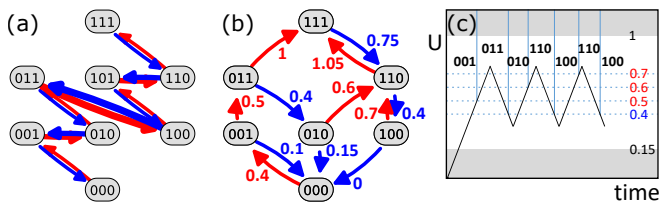


FIG. 4. (a) T-graph that sequentially accesses states by sweeping U . (b) Accumulator t-graph with switching fields as indicated. (c) Response demonstrating that for $0.7 < U_M < 1$, states $\{110\}$ and $\{100\}$ are only reached after two driving cycles. Dashed lines indicate critical switching fields, and grey regions indicate potential transitions to the extremal states.

dered binary numbers 000-111 (Fig. 4(a)). The design inequalities specify a linear programming problem [25], and a judicious choice of parameters allows to tune the critical switching fields of the seven up and seven down transitions exactly to values $0.1, 0.2, \dots, 0.7$, respectively $0.65, 0.55, \dots, 0.05$, making all states easily addressable (see Supplemental Information).

As a second example, we explore the breakdown of l-RPM and select an ‘accumulator’ t-graph that contains the pathway $\{001\} \uparrow \{011\} \downarrow \{010\} \uparrow \{110\} \downarrow \{100\}$ (Fig. 4(b)-(c)). We choose parameters such that the two down transitions occur at $U = 0.4$, and the three up transitions occur at respective switching fields $0.5, 0.6$ and 0.7 (Fig. 4b). The response of this system when U is cycled between $u_m > 0.15$ and $u_M < 1$ evidences counting behavior. For $0.7 < U_M < 1$, the system reaches state $\{011\}$ at the first peak, and state $\{110\}$ at subsequent peaks: this pathway distinguishes between one or more cyclical drivings (Fig. 4c). Such response has recently been observed in experiments on crumpled sheets [13]. Moreover, for $0.6 < U_M < 0.7$, the first cycle reaches $\{011\}$, the second $\{110\}$ and subsequent cycles remain stuck at $\{100\}$ (“counting to three”); for $0.5 < U_M < 0.6$, the first cycle reaches $\{011\}$ and subsequent cycles remain stuck at $\{010\}$. Hence, such a collection of hysterons can count to two or three, depending on driving amplitude.

A variety of more complex functions may be achievable in t-graphs that encode longer S-cycles, multiple S-cycles, etc. Moreover, we note that for the same t-graph topology, different parameters that, e.g., tune all relevant up transition fields to the same value, can achieve qualitatively different behaviors (see Supplemental Information). Hence, the design space for complex hysteron “machines” is very large.

Discussion. — This work highlights that even small collections of weakly interacting hysterons exhibit a staggering multitude and variety of pathways and t-graphs, and suggests that hysterons with appropriate thresholds and interactions can act as information processing devices. We highlight a number of key questions. First, the

types of t-graphs and underlying computations that can be realized by interacting hysterons is unknown, with interesting sub-questions arising for interactions that are purely ferromagnetic, purely antiferromagnetic, reciprocal ($c_{ij} = c_{ji}$ [25]), or sparse. Second, in exploratory studies we have found that the fraction of random parameters that yield ill-defined t-graphs increases with n and C and asymptotes to one. This suggests that strongly coupled systems cannot always be described by hysterons, and more advanced models, that avoid ambiguities due to multiple unstable hysterons or self-loops, are called for. Third, metamaterials might yield physical realizations, with serially coupled mechanical hysterons naturally implementing anti-ferromagnetic interactions [27, 31, 36]. Finally, viscoelastic effects could be leveraged to obtain rate-dependent pathways and t-graphs and self-learning systems [37–41]. Together, progress on these questions will realize targeted pathways and information processing in designer materials.

Acknowledgements. — We acknowledge insightful discussions with H. Bense, K. Bertoldi, N. Keim, G. Korovin, Y. Lahini, C. Lindeman, M. Mungan, S. Nagel, J. Paulsen and M. Zanaty.

-
- [1] E.M. Kramer and T.A. Witten, Phys. Rev. Lett. **78**, 1303 (1997).
 - [2] E. Cerda, S. Chaieb, F. Melo, and L. Mahadevan, Nature **401**, 46 (1999).
 - [3] K. Matan, R. B. Williams, T. A. Witten and S. R. Nagel, Phys. Rev. Lett. **88**, 076101 (2002).
 - [4] T. A. Witten, Rev. Mod. Phys. **79**, 643 (2007).
 - [5] H. Aharoni and E. Sharon, Nat. Mater. **9**, 993 (2010).
 - [6] N. Oppenheimer and T. A. Witten, Phys. Rev. E **92**, 052401 (2015).
 - [7] Y. Lahini, O. Gottesman, A. Amir and S. M. Rubinstein, Phys. Rev. Lett. **118**, 085501 (2017).
 - [8] K. A. Murphy, J. W. Kruppe and H. M. Jaeger, Phys. Rev. Lett. **124**, 168002 (2020).
 - [9] R. Candelier and O. Dauchot, Phys. Rev. Lett. **103**, 128001 (2009).
 - [10] S. Slotterback, M. Mailman, K. Ronaszegi, M. van Hecke, M. Girvan and W. Losert, Phys. Rev. E **85** 021309 (2012).
 - [11] N. C. Keim and S. R. Nagel, Phys. Rev. Lett. **107**, 010603 (2011).
 - [12] D. Bonn, M. M. Denn, L. Berthier, T. Divoux and S. Manneville, Rev. Mod. Phys. **89**, 035005 (2017).
 - [13] H. Bense and M. van Hecke, arXiv:2106.14441 (2021).
 - [14] J. P. Sethna, K. A. Dahmen and C. R. Myers, Nature **410**, 242 (2001).
 - [15] F. Preisach, Z. Physik **94**, 277 (1935).
 - [16] J. A. Barker, D. E. Schreiber, B. G. Huth and D. H. Everett, Proc. Roy. Soc. A **386**, 251 (1983).
 - [17] A. A. Middleton, Phys. Rev. Lett. **68**, 670 (1992).
 - [18] J. P. Sethna, K. Dahmen, S. Kartha, J. A. Krumhansl, B. W. Roberts and J. D. Shore, Phys. Rev. Lett. **70**, 3347 (1993).

- [19] N. C. Keim, J. D. Paulsen, Z. Zeravcic, S. Sastry, and S. R. Nagel, *Rev. Mod. Phys.* **91**, 035002 (2019).
- [20] M. Mungan and M. Mert, *Ann. H. Poincare* **20**, 2819 (2019).
- [21] M. M. Terzi and M. Mungan, *Phys. Rev. E* **102**, 012122 (2020).
- [22] M. Mungan, S. Sastry, K. Dahmen and I. Regev, *Phys. Rev. Lett.* **123**, 178002 (2019).
- [23] I. Regev, I. Attia, K. Dahmen, S. Sastry, M. Mungan, arXiv:2101.01083 (2021).
- [24] J. D. Paulsen and N. C. Keim, *Proc. Roy. Soc. A* **475**, 20180874 (2019).
- [25] N. C. Keim and J. D. Paulsen, arXiv:2101.01240 (2021).
- [26] C. W. Lindeman and S. R. Nagel, arXiv:2101.01632 (2021).
- [27] T. Jules, A. Reid, K. E. Daniels, M. Mungan, F. Lechenault, arXiv:2106.08243 (2021).
- [28] K. Bertoldi, V. Vitelli, J. Christensen and M. van Hecke, *Nat. Rev. Mat.* **2**, 17066 (2017).
- [29] C. Coulais, A. Sabbadini, F. Vink and M. van Hecke, *Nature* **561**, 512 (2018).
- [30] M. Stern, V. Jayaram, and A. Murugan, *Nat. Comm.* **9**, 4303 (2018).
- [31] M. Zanaty and K. Bertoldi, *Private Comm.*
- [32] Nonzero diagonal interaction constants c_{ii} only affect the values of U_i^- and can readily be absorbed in the bare switching fields u_i^- .
- [33] We assume no degeneracies to occur.
- [34] The multi-edges in antiferromagnetic multigraphs feature pairs of 'horizontal' avalanches only.
- [35] J. Sakavorith, *Elements of automata theory*, Cambr. Univ. Press London, (2009).
- [36] J. Liu, G. Korovin, Z. Vermaire, H. Bense and M. van Hecke, *in prep.*
- [37] D. Dykstra, J. Busink B. Ennis and C. Coulais, *J. App. Mech.* bf 86 111012 (2019).
- [38] S. Janbaz, K. Narooei, T. van Manen and A. A. Zadpoor, *Science Advances* **6**, eaba0616 (2020).
- [39] A. Bossart, D. M. J. Dykstra, J. van der Laan and C. Coulais, *PNAS* **118**, e2018610118 (2021).
- [40] N. Pashine, D. Hexner, A. J. Liu and S. R. Nagel, *Sci. Adv.* **5**, eaax4215 (2019).
- [41] M. Stern, D. Hexner, J. W. Rocks and A. J. Liu, *Phys Rev X* **11**, 021045 (2021).

SUPPLEMENTARY INFORMATION

I. MODEL

The model used in this paper linearly couples hysterons. We first consider the nature of its transitions. The upper and lower switching fields for state S are

$$U^+(S) = \min_{i_0} U_{i_0}^+(S) , \quad (1)$$

$$U^-(S) = \max_{i_1} U_{i_1}^-(S) , \quad (2)$$

where i_0 (i_1) runs over the hysterons that are 0 (1). State S becomes unstable when U exceeds $U^+(S)$ or decreases below $U^-(S)$, initiating an up resp. down transition at critical driving value $U^c = U^\pm(S)$ and defining a transition state S' . By considering the stability of all hysterons in this transition state S' at $U = U^c$, four distinct scenario's can arise (Fig. 1). (i) The transition state S' is a stable landing state when $U^-(S') < U^c < U^+(S')$ yielding a transition between state S and S' (Fig. 1(a)). While S' is always stable at $U = U^c$ when $c_{ij} = 0$, interactions may cause state S' to be unstable, leading to avalanches. (ii) When one '0' hysteron of S' is unstable, there is an additional up transition from S' to S'' (Fig. 1(b)), while when one '1' hysteron is unstable, there is an additional down transition from S' to S''' (Fig. 1(c)). If state S'' is stable, we obtain an avalanche of length two between state S and S'' in which two hysterons change their phase at fixed $U = U^c$; if state S''' is unstable, we iterate and may find longer avalanches. (iii) Occasionally more than one hysteron may be unstable in a given state (Fig. 1(d)). We have observed that such conditions can arise for arbitrarily weak interactions. Extensions of the model could be considered so that the 'most unstable' hysteron would switch and define state S'' —here we choose to consider the corresponding t-graph to be ill-defined whenever such a condition arises.

A. Recursive Algorithm

We collect transitions between states that can be reached from the ground state $\mathbf{0} = \{0, 0, \dots\}$ into a t-graph via an iterative algorithm. This algorithm initiates a t-graph by node $\mathbf{0}$ and determines its up transition to a state S_1 following the procedure outlined above. Node S_1 is then added to the graph, as well as the edge $\mathbf{0} \rightarrow S_1$. Node $\mathbf{0}$ is then labeled as 'stale', as all its transitions have been determined, and S_1 is labeled as a 'fresh' node. The up (provided $S_1 \neq \mathbf{1} = \{1, 1, \dots\}$) and down transitions from the fresh state S_1 to states S_2 and S_3 are determined, state S_1 is labeled as stale, and states S_2 and S_3 are added to the t-graph and labeled as fresh provided they have not been visited before. This procedure is repeated until no more new fresh states are found.

Occasionally, loop-like avalanches of the form $S \rightarrow S' \dots \rightarrow S$ occur: we consider the corresponding t-graphs ill-defined. We suggest that more elaborate models, which for example would have an energy functional and dissipation, could be constructed to avoid such self-loops.

The resulting t-graph contains all N nodes that are connected to state $\mathbf{0}$ and the $2N - 2$ directed edges which represents the transitions, where each edge is labeled by its character (up or down transition), its corresponding critical field U^c , and its length, i.e., the number of steps in an avalanche (one for an ordinary transition). Graphically, we order the nodes from bottom to top as function of their magnetization $m = \sum s_i$, and from left to right lexicographically. Up and down transitions are colored red and blue, and the thickness of the edges represents the length of the avalanche.

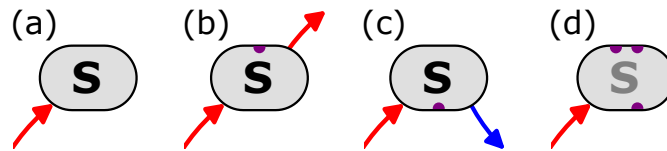


FIG. 1. Four scenario's after an up-transition reaches the state S at $U = U^c$ (red incoming arrow), depending on the stability of each hysteron in state S at $U = U^c$; unstable hysterons in the 0 (1) phase are visualized as purple dots at the top (bottom) of the node S . (a) The transition terminates at S when all hysterons are stable at $U = U^c$. (b) If one phase 0 hysteron is unstable at $U = U^c$, this hysteron switches to phase 1, defining an additional step of the transition that now forms an avalanche (red outgoing arrow). (c) If one phase 1 hysteron is unstable at $U = U^c$, this hysteron switches to phase 0, defining an additional step of the transition that now forms an avalanche (blue outgoing arrow). (d) If more than one hysteron is unstable at $U = U^c$, we consider the model ill-defined.

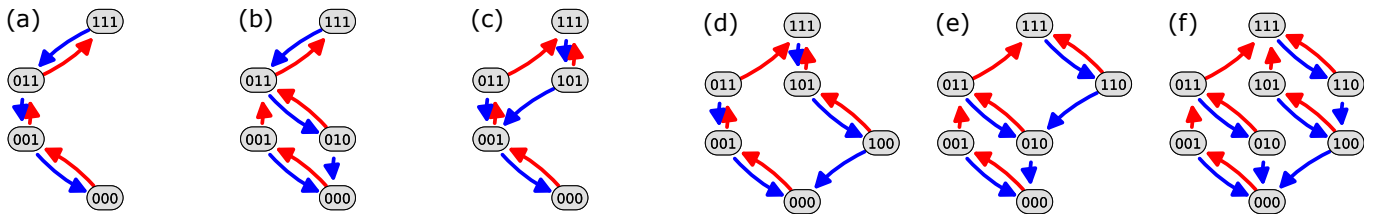


FIG. 2. T-graphs for the $n = 3$ Preisach model (no interactions), for $u_1^+ > u_2^+ > u_3^+$. The ordering of the lower switching fields determines each graph [21,22]: (a) $u_1^- > u_2^- > u_3^-$. (b) $u_1^- > u_3^- > u_2^-$. (c) $u_2^- > u_1^- > u_3^-$. (d) $u_2^- > u_3^- > u_1^-$. (e) $u_3^- > u_1^- > u_2^-$. (f) $u_3^- > u_2^- > u_1^-$.

B. Preisach t-graphs

In the absence of interactions, the model is exactly the Preisach model, whose t-graphs and properties have recently received renewed attention. Under the assumed ordering of the upper switching fields, each permutation of the ordering of the lower switching fields yields a unique t-graph, that we include here (for $n = 3$) for completeness (Fig. 2). We note that the two $n = 2$ Preisach t-graphs are equivalent to the subgraphs of Fig. 2 obtained by pruning the $\{11x\}$ states.

C. Numerical sampling of design space

While the interactions constants c_{ij} are flatly sampled, only restricted by simple independent constraints such as $|c_{ij}| < C$, the bare switching fields have to satisfy two sets of constraints: First, we require $u_i^- < u_i^+$ so that independent hysterons are well-defined, and second, we require the ordering of the upper switching fields ($u_1^+ > u_2^+ > \dots$) which limits the number of t-graphs by suppressing trivial permutations of the hysterons. To numerically sample the switching fields that satisfy these constraints, we use an algorithm that guarantees that, for $c_{ij} \equiv 0$, all different orderings of the lower switching fields, and thus all Preisach t-graphs, occur with equal probability.

II. DESIGN EQUATIONS

Here we provide the full set of conditions on the design parameters u_i^\pm, c_{12} and c_{21} for each of the 11 t-graphs of $n = 2$ interacting hysterons, as shown in Fig. 2(a)-2(k) of the main text. We moreover discuss how these give rise to the powerlaw scaling shown in Fig. 2(l) of the main text.

A. Design inequalities for $n = 2$ interacting hysterons

We recall the following design constraints on the bare switching fields:

$$u_2^+ < u_1^+, \quad (3)$$

$$u_1^- < u_1^+, \quad (4)$$

$$u_2^- < u_2^+. \quad (5)$$

To systematically determine the conditions for all potential $(2 \cdot 2^n - 2)$ up and down transitions, we first determine the $n \cdot 2^n$ switching fields of each hysteron (Fig. 3a). We then choose an initial state S and proceed via a three step process: (i): We determine the conditions for the switching hysteron and the concomitant switching field $U^c(S)$. (We note that while for $n = 2$ only the down transition from state $\{11\}$ yields a non-trivial condition, for larger n the situation is more elaborate.) (ii): We consider the stability conditions of the transition state S' at U^c . If S' is stable, it is a landing state, and we have found an $S \rightarrow S'$ transition. (iii): When one stability condition for S' is not met it is unstable, an avalanche occurs with a new switching hysteron and towards the next transition state S' — the critical U remains as determined in the first step. For this new state, we repeat step (ii)-(iii). When more than one stability condition is not met, the avalanche is ill-defined. Similarly, when $S' = S$, the system is ill-defined as this causes a loop.

Starting out at state S , these three steps yield a set of inequalities for all transitions starting out at S which span a decision tree. We note that the number of inequalities quickly grows with the number of steps in an avalanche (i.e.,

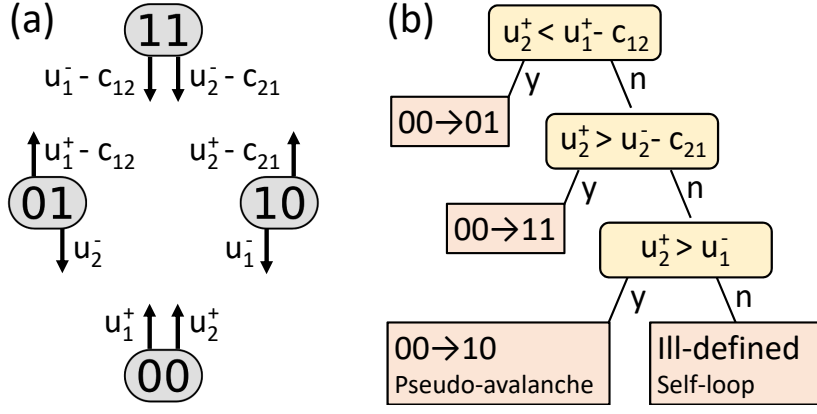


FIG. 3. (a) Switching fields of each hysteron in each potential state of two interacting hysterons. Up and won arrows indicate up and down transitions; left and right positioning indicates switching fields for hysteron 1 and 2, respectively. (b) Decision tree summarizing the conditions for transitions starting from state $\{00\}$.

deeper into the three) and also with the number of hysterons, consistent with the explosive growth in the variety of t-graphs with n . Repeating this exercise for all states S , and collecting the inequalities in all corresponding threes, while tedious, yields a complete set of necessary and sufficient conditions on the design parameters for each t-graph, as well as conditions for the t-graph to be ill-defined.

Example. — To illustrate this approach, we explicitly consider the up transitions from state $\{00\}$ towards all other states following the three step process. (i): The design constraint Eq. (3) determines that the 2nd hysteron will switch, so that $U^c = u_2^+$, and $S' = \{01\}$. (ii) For S' to be stable at U^c , we require:

$$U^c = u_2^+ < u_1^+ - c_{12} , \quad (6)$$

$$U^c = u_2^+ > u_2^- , \quad (7)$$

where we note that the second condition is trivially satisfied due to the design constraint Eq. (5). Hence we can conclude the following necessary and sufficient condition:

$$\{00\} \rightarrow \{01\} : u_2^+ < u_1^+ - c_{12} . \quad (8)$$

We note that for non-interacting hysterons, where $c_{12} = 0$, this condition is trivially satisfied due to design condition Eq. (3). Moreover, this constraint can only be violated for positive $c_{12} > u_2^+ - u_1^+$. More generally, "vertical" and "horizontal" avalanches require positive and negative coupling coefficients.

We now iterate this process, by considering the case when the transition state $\{01\}$ is not stable, i.e. when Eq. (8) is not satisfied. We then obtain a new transition state $S' = \{11\}$, and we check the stability of S' :

$$u_2^+ > u_1^- - c_{12} , \quad (9)$$

$$u_2^+ > u_2^- - c_{21} . \quad (10)$$

We note that Eq. (9) is automatically satisfied because of the design constraint Eq. (4) and the fact that Eq. (8) is not satisfied. Inequality (9) is thus redundant and can be removed from our considerations - such dependencies between inequalities on the design parameters frequently occur. Hence, the necessary conditions for an avalanche from $\{00\}$ to $\{11\}$ are:

$$\{00\} \rightarrow \{11\} : \quad (11)$$

$$u_2^+ > u_1^+ - c_{12} , \quad (11)$$

$$u_2^+ > u_2^- - c_{21} . \quad (12)$$

We now consider whether these equations are sufficient. For an avalanche, we do not keep track of the intermediate transition states and only monitor the initial and final state. In principle, the $\{00\} \rightarrow \{11\}$ avalanche might also have proceeded differently, e.g., via the $\{10\}$ state; in this specific case, the design constraint Eq. 3 blocks this possibility. For larger systems, finding sufficient and necessary conditions for avalanches becomes much more involved. However, in this specific case, Eqs. (11) and (12) are both sufficient and necessary conditions for the $\{00\} \rightarrow \{11\}$ avalanche.

We repeat this procedure again in case that state $\{11\}$ is unstable at $U = u_2^+$, which happens when Eq. (11) is satisfied, and Eq. (12) is violated, and which leads to a new transition state $\{10\}$. Checking the stability of this state yields:

$$u_2^+ < u_2^+ - c_{21} , \quad (13)$$

$$u_2^+ > u_1^- . \quad (14)$$

$$(15)$$

We note that c_{21} has to be negative to violate Eq. (12), which implies that Eq. (13) is satisfied and can be removed from our consideration. Hence, the conditions for the pseudo avalanche of length three $\{00\} \rightarrow \{10\}$ of t-graph (j) (see Fig. 2 main text) are:

$$\{00\} \rightarrow \{10\} : \quad u_2^+ > u_1^+ - c_{12} , \quad (16)$$

$$u_2^+ < u_2^- - c_{21} , \quad (17)$$

$$u_2^+ > u_1^- . \quad (18)$$

Finally, we note that violating the last equality Eq. (18) yields a cycle $\{00\} \rightarrow \{00\}$, which yields the t-graph to be ill-defined; this indeed can happen (a concrete realization would be $u_1^+ = 0.5, u_1^- = 0.8, u_2^+ = 1, u_2^- = 0.7, c_{12} = 0.1, c_{21} = -0.4$). We summarize these findings in a decision tree (Fig. 1b), where we stress that for other states and for more hysterons, the situation generally is much more complex, featuring multiple conditions and outcomes per branch point, and cases where different branches yield the same transition.

After collecting all inequalities for all possible $n = 2$ transitions, and removing redundant inequalities, we obtain necessary and sufficient conditions for each of the 11 possible t-graphs, as well as precise conditions for the occurrence of ill-defined graphs. We can express these by combining nine inequalities x_i , and we have checked these conditions numerically. We note that these inequalities x_i are not independent - for example, $x_1 \wedge x_8 \Rightarrow x_7$ - and we have checked that only 78 different combinations of $\{x_1, \dots, x_9\}$ arise.

t-graph	Condition	Condition
(a)	$\neg x_1 \wedge \neg x_3 \wedge \neg x_4 \wedge x_6 \wedge x_7$	$\begin{array}{cccc c} x_1 & -u_1^+ & +u_2^+ & +c_{12} & > 0 \\ x_2 & & -u_1^- & +u_2^- +c_{12} & > 0 \\ x_3 & & +u_1^- & -u_2^- -c_{12} +c_{21} & > 0 \\ x_4 & & +u_1^- & -u_2^- & +c_{21} > 0 \\ x_5 & & & -u_2^+ +u_2^- & -c_{21} > 0 \\ x_6 & +u_1^+ & & -u_2^- -c_{12} +c_{21} & > 0 \\ x_7 & & -u_1^- +u_2^+ & & > 0 \\ x_8 & +u_1^+ & -u_1^- & -c_{12} & > 0 \\ x_9 & & +u_1^- & -u_2^+ & -c_{12} > 0 \end{array}$
(b)	$\neg x_1 \wedge \neg x_2 \wedge x_3 \wedge x_6$	
(c)	$\neg x_1 \wedge \neg x_3 \wedge \neg x_4 \wedge \neg x_6 \wedge x_7 \wedge x_8$	
(d)	$\neg x_1 \wedge \neg x_3 \wedge \neg x_4 \wedge x_6 \wedge \neg x_7 \wedge x_8$	
(e)	$\neg x_1 \wedge \neg x_3 \wedge \neg x_4 \wedge \neg x_6 \wedge \neg x_7 \wedge x_8$	
(f)	$\neg x_1 \wedge ((x_2 \wedge x_3) \vee (\neg x_3 \wedge x_4)) \wedge \neg x_5$	
(g)	$x_1 \wedge \neg x_2 \wedge x_3 \wedge \neg x_5 \wedge x_6 \wedge \neg x_9$	
(h)	$x_1 \wedge \neg x_3 \wedge \neg x_4 \wedge \neg x_5 \wedge x_7 \wedge \neg x_9$	
(i)	$x_1 \wedge ((x_2 \wedge x_3) \vee (\neg x_3 \wedge x_4)) \wedge \neg x_5$	
(j)	$x_1 \wedge \neg x_3 \wedge \neg x_4 \wedge x_5 \wedge x_7$	
(k)	$\neg x_1 \wedge \neg x_3 \wedge x_4 \wedge x_5 \wedge x_6$	
ill	$\neg x_3 \wedge x_5 \wedge \neg x_6 \wedge \neg x_7 \wedge \neg x_8$	

TABLE I. Left: Necessary and sufficient conditions for each $n = 2$ t-graph (a)-(k), and for ill-defined t-graphs. Right: Nine conditions x_i on the design parameters.

B. Power law scaling

We note that the fact that each type of t-graph requires a set of inequalities also underpins the power law scaling of their probability in random samples as a function of $|C|$ (Fig. 2l main text). For example, consider condition $x_1 : u_2^+ - u_1^+ > -c_{12}$. As the design constraint Eq. (3) stipulates that $u_2^+ < u_1^+$, x_1 can only be satisfied when c_{12} is positive, and when $c_{12} \downarrow 0$ requires the difference between u_1^+ and u_2^+ to become vanishingly small, which statistically happens with probability $\mathcal{O}(|c|)$ - hence, x_1 is a critical condition for small $|c|$. Similarly, conditions $x_5, \neg x_6$ and $\neg x_8$ also are satisfied with probability $\mathcal{O}(|c|)$. Moreover, some combinations of condition may only occur with probability $\mathcal{O}(|c|)$. When m independent critical conditions occur, t-graphs can only arise with probability $\mathcal{O}(|c|^m)$. Similarly, when $|c|$ becomes very large, some (combinations) of the inequalities x_i can only be satisfied when the coupling constants are of order one, which happens with probability $\mathcal{O}(|c|^{-1})$. Together, these considerations explain the power law behavior seen in Fig. 2l of the main text.

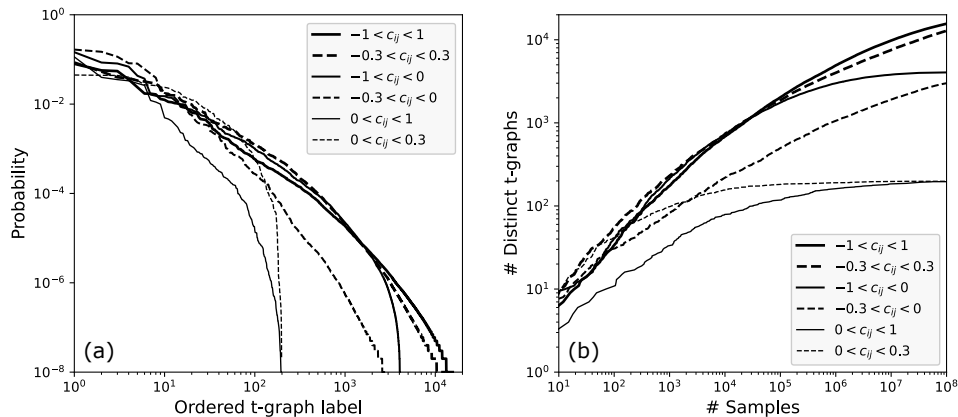


FIG. 4. Statistical measures of $n = 3$ t-graphs, for two different interactions strengths and for mixed, ferromagnetic, and purely anti-ferromagnetic interactions.

III. CLASSES OF T-GRAPHS

A. Scrambling

We note that in the main text we defined scrambling only for t-graphs without avalanches. This is because when avalanches are present, their intermediate steps are "hidden" but would still be required to understand whether a given avalanche is scrambled with respect to other transitions. Of course, this does not rule out that two direct (i.e. length one) transitions are scrambled in a t-graph that also contains avalanches — see for example Fig. 3g in the main text.

B. Definition of l-RPM

Define operators U and D so that $U(S)$ (and $D(S)$) produces the state after an up (down) transition from state S , and define the full up orbit $Up(S)$ as the sequence of states $U(s), U^2(s), \dots$, and similarly for the down orbit $Dw(S)$. Consider a loop, defined by a pair of states S_m and S_M , such that the system evolves from S_m to S_M (and vice-versa) by a series of exclusively up (down) transitions. Define the up boundary of a loop as the sequence of states obtained by repeatedly applying U on S_m until S_M is reached, and the down boundary as the sequence of states by applying D on S_M until S_m is reached. A loop is said to be absorbing if the states S_m (S_M) are part of the down (up) orbit from any state which is part of the up (down) boundary—this implies that the system can only escape a subloop through the extremal states. A t-graph has the l-RPM property if and only if all loops are absorbing [21,22].

IV. STATISTICS $n=3$ T-GRAPHS

In Fig. 4 we show additional statistical measures for our ensembles of $n = 3$ t-graphs, for interactions strengths $C = 0.3$ and $C = 1$ and for mixed ($-C < c_{ij} < C$), ferromagnetic ($0 < c_{ij} < C$), and purely anti-ferromagnetic ($-C < c_{ij} < 0$) interactions. For each ensemble we sample 10^8 parameter values. We order each t-graph by its probability (from high to low), and observe that the probabilities for a given t-graph span many decades, with the majority of t-graphs spanning a small fraction of parameter space (Fig. 4(a)). Second, we observe that the number of distinct t-graphs as function of the number of samples grows slowly, and with slightly different rates depending on the interaction strength and qualitative character; moreover, while for 10^8 realizations the number of t-graphs for purely ferromagnetic and antiferromagnetic appears has (nearly) saturated around 198 and $\mathcal{O}(4050)$, the number of t-graphs for mixed interactions is still growing (Fig. 4(b)).

Panel	u_1^+	u_2^+	u_3^+	u_1^-	u_2^-	u_3^-	c_{12}	c_{13}	c_{21}	c_{23}	c_{31}	c_{32}
(a)	0.9	0.6	0.5	0.2	0.4	0.1	0	0	0	0	-0.2	-0.2
(b)	1	0.8	0.6	0.55	0	0.4	-0.1	-0.4	-0.75	-0.45	-0.4	-0.45
(c)	1	0.9	0.8	0.2	0.8	0	0	0	0	-0.15	-0.3	0
(d)	1	0.7	0.5	0.3	0.6	0.4	0.0	-0.15	0	0.25	0	0
(e)	1	0.9	0.8	0.3	0.2	0.5	0.25	-0.2	0	0.2	0	0
(f)	0.9	0.7	0.6	0	0.1	0.3	0.1	-0.3	0.3	-0.25	0	-0.6
(g)	0.9	0.7	0.5	0.1	0.4	0.35	0.3	-0.4	-0.7	0	-0.7	0.1
(h)	1	0.95	0.9	0.55	0.6	0.7	0.23	-0.3	0.1	0.4	0.3	-0.18
(i)	0.75	0.6	0.3	0.35	0.39	0.28	-0.05	-0.30	0	-0.4	0.05	-0.6

TABLE II. Examples of switching fields and coupling coefficients that produce the t-graphs shown in Fig. 3 of the main text.

V. SPECIFIC DESIGNS

Here we tabulate specific values of the switching fields and interaction constants that produce the t-graphs seen in Fig. 3 and Fig. 4 from the main text, as well as summarize some more details about their designs and properties.

A. Specific designs for Fig. 3

In table II we present examples of switching fields and coupling coefficients that produce t-graphs with the same topologies as shown in Fig. 3 of the main text. These parameter values have been selected after some manual optimization steps, setting some small interactions to zero and rounding of all values to at most two significant digits. While these parameters are not optimal in any well-defined sense, they may serve as specific starting points for further studies, as well as to guide the reader in the construction of t-graphs by providing few specific examples. Moreover, we have numerically checked that for these parameters, small changes of $\mathcal{O}(10^{-3})$ do not change the topology of the t-graph, thus demonstrating that even rare graphs are robust.

B. Properties and pathways t-graphs in Fig. 3.

Here we summarize the specific properties and pathways (in particular, S-cycles and orbits that break l-RPM) of the t-graphs in Fig. 3 of the main text.

Panel (a): This t-graph has no cycles and satisfies l-RPM.

Panel (b): This t-graph has a subharmonic cycle: $\{001\} \uparrow \{011\} \uparrow \{111\} \downarrow \{110\} \downarrow \{100\} \uparrow \{101\} \downarrow \{001\} \dots$ where \uparrow and \downarrow denote up and down transitions. Moreover, it breaks l-RPM. To see this, consider the sub-loop between nodes $S_m = \{100\}$ and $S_M = \{111\}$. Node $\{101\}$ is part of the up boundary. However, its down orbit, $\{101\} \rightarrow \{001\} \rightarrow \{000\}$ never reaches its S_m . Hence, this loop is not absorbing, and the t-graphs does not have the l-RPM property. In more compact notation: $[S_m, S_M] = [\{100\}, \{111\}]; \{101\} \in \text{up boundary}; S_m \notin Dw(\{101\})$.

Panel (c): This t-graphs does not have an S-cycle, yet breaks l-RPM: $[S_m, S_M] = [\{000\}, \{101\}]; \{100\} \in \text{down boundary}; S_M \notin Up(\{100\})$.

Panel (d): This t-graph contains two avalanches of length two, no S-cycles, and satisfies l-RPM.

Panel (e): This t-graph has an S-cycle: $\{000\} \uparrow \{011\} \downarrow \{010\} \uparrow \{110\} \downarrow \{000\} \dots$. It also breaks l-RPM: $[S_m, S_M] = [\{000\}, \{011\}]; \{010\} \in \text{down boundary}; S_M \notin Up(\{010\})$.

Panel (f): This t-graph contains no S-cycles, yet breaks l-RPM: $[S_m, S_M] = [\{000\}, \{011\}]; \{110\} \in \text{down boundary}; S_M \notin Up(\{110\})$.

Panel (g): This t-graph has no cycles and satisfies l-RPM. We note that the simultaneous presence of the transitions $\{001\} \rightarrow \{011\}$ and $\{100\} \rightarrow \{101\}$ indicates scrambling.

Panel (h): This t-graph contains a S-cycle: $\{000\} \uparrow \{011\} \uparrow \{111\} \downarrow \{010\} \uparrow \{110\} \downarrow \{000\} \dots$. Moreover, this t-graph contains several orbits that violate l-RPM. For sub-loop $[S_m, S_M] = [\{000\}, \{011\}]$, states $\{111\}$ and $\{010\}$ are part of the down boundary, but neither of their up orbits reach S_M ; moreover for sub-loop $[S_m, S_M] = [\{010\}, \{111\}]$, state $\{110\} \in \text{up boundary}$, while $S_m \notin Dw(\{110\})$.

Panel (i): This t-graph has no S-cycles yet many examples of orbits that violate l-RPM. For the sub-loop $[S_m, S_M] = [\{000\}, \{011\}]$, states $\{111\}$, $\{110\}$ and $\{010\}$ are parts of the down boundary, yet their up orbits do not reach S_M .

Panel	u_1^+	u_2^+	u_3^+	u_1^-	u_1^-	u_1^-	c_{12}	c_{13}	c_{21}	c_{23}	c_{31}	c_{32}
(a)	0.8	0.4	0.1	0.35	0.15	0.05	0	0	0	0	-0.2	-0.2
(b)	0.7	0.45	0.4	0	0.15	0.1	0.1	-0.4	-0.25	-0.05	-0.35	-0.3
(x)	0.7	0.45	0.42	0	0.255	0.08	0.1	-0.4	-0.15	0	-0.15	-0.25

TABLE III. Examples of switching fields and coupling coefficients that produce the t-graphs shown in Fig. 4 of the main text (a,b) and an alternative design (x).

Moreover, also for sub-loop $[S_m, S_M] = [\{001\}, \{011\}]$, states $\{111\}$, $\{110\}$ and $\{010\}$ are parts of the down boundary, yet none of their up orbits reach S_M .

C. Specific designs for Fig. 4

In table III we present examples of switching fields and coupling coefficients that produce t-graphs with the same topologies as shown in Fig. 4 of the main text, as well as for an additional design shown in Fig. 5 below.

Panel (a): For the example parameters shown in Table. III(a), the critical switching fields of the seven up transitions from state $\{000\} \rightarrow \{001\} \dots$ are equal to $0.1, 0.2, \dots, 0.7$, and the critical switching fields of the seven down transitions from state $\{111\} \rightarrow \{110\} \dots$ are equal to $0.65, 0.55, \dots, 0.05$. We have in addition verified that the t-graph's topology is stable to random perturbations of the design parameters of magnitude 10^{-3} .

Panel (b): For the example parameters shown in Table. III(b), the critical switching fields are as shown in Fig. 4b of the main text. In particular, the switching fields for $\{011\} \downarrow \{010\}$ and $\{110\} \downarrow \{100\}$ are equal to 0.4 , while the switching fields for $\{001\} \uparrow \{011\}$, $\{010\} \uparrow \{110\}$, and $\{100\} \uparrow \{110\}$ are equal to $0.5, 0.6$ and 0.7 , respectively. We have verified that the t-graph's topology is stable to random perturbations of the design parameters of magnitude 10^{-3} . We consider driving where U is swept up from zero to u_m , and then cycled between $u_m < u_M$. As long as $U_m > 0.15$ and $U_M < 1$, the extremal states $\mathbf{0}$ and $\mathbf{1}$ are not reached. Then, the response of the system depends on the value of U_M as indicated in the main text.

Alternative design: The free parameters in our model offer freedom in the choice of the critical switching fields, although there are some constraints. For example, requiring that all three relevant up transitions in the accumulator t-graph ($\{001\} \uparrow \{011\}$, $\{010\} \uparrow \{110\}$, $\{100\} \uparrow \{110\}$) are equal necessitates the two down transitions ($\{011\} \downarrow \{010\}$, $\{110\} \downarrow \{100\}$) to be unequal. To see this, we notice that in terms of the design parameters, the three up transitions are at $u_2^+ - c_{23}, u_1^+ - c_{12}$ and $u_2^+ - c_{21}$ respectively, so that when all are equal, $c_{21} = c_{23}$. Similarly, for the down transitions to have equal switching fields, we require $u_3^- - c_{32} = u_2^- - c_{21}$. Finally, for the down transition from state $\{011\}$ land on state $\{010\}$ and not on $\{001\}$, we require the design inequality $u_3^- - c_{32} > u_2^- - c_{23}$. When the pair of down transitions are equal, this latter inequality can be rewritten as $u_2^- - c_{21} > u_2^- - c_{23} \Rightarrow c_{21} < c_{23}$, which is in disagreement with the requirement that all three up transitions are at the same switching field.

It is however easy to find design parameters to that the three up-transitions are equal (Table. III(x)), yielding the critical switching fields shown in Fig. 5. As all the relevant up switching fields are equal, the only behavior that is left is "counting to two", demonstrating that even for a given t-graph topology, qualitatively distinct responses and finite state machines may be encoded.

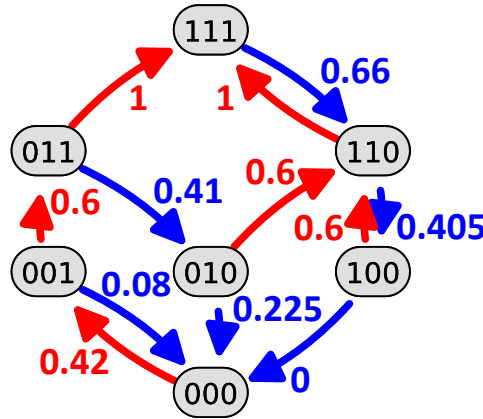


FIG. 5. Switching fields corresponding to an alternative design for the accumulator (Table III(x)).